

Analysis of the layering pattern of the apparent diffusion coefficient (ADC) for differentiation of radiation necrosis from tumour progression

Jihoon Cha · Sung Tae Kim · Hyung-Jin Kim ·
Hye Jeong Kim · Byung-joon Kim · Pyoung Jeon ·
Keon Ha Kim · Hong Sik Byun

Received: 11 April 2012 / Revised: 17 July 2012 / Accepted: 1 August 2012 / Published online: 19 August 2012
© European Society of Radiology 2012

Abstract

Objectives To evaluate the added value of diffusion-weighted imaging (DWI) to perfusion-weighted imaging (PWI) for differentiating tumour progression from radiation necrosis.

Methods Sixteen consecutive patients who underwent removal of a metastatic brain tumour that increased in size after stereotactic radiosurgery were retrospectively reviewed. The layering of the ADC was categorised into three patterns. ADC values were measured on each layer, and the maximum rCBV was measured. rCBV and the layering pattern of the ADC of radiation necrosis and tumour progression were compared.

Results Nine cases of radiation necrosis and seven cases of tumour progression were pathologically confirmed. Radiation necrosis (88.9 % vs. 14.3 %) showed a three-layer pattern of ADC with a middle layer of minimum ADC more frequently. If rCBV larger than 2.6 was used to differentiate radiation necrosis and tumour progression, the sensitivity was 100 % but specificity was 56 %. If the lesions with the three-layer pattern of ADC with moderately increased rCBV (2.6–4.1) were excluded from tumour progression, the sensitivity and specificity increased to 100 %.

Conclusions The three-layer pattern of ADC shows high specificity in diagnosing radiation necrosis; therefore, combined analysis of the ADC pattern with rCBV may have added value in the correct differentiation of tumour progression from radiation necrosis.

Key Points

- MRI follow-up often reveals increasing size of enhancing lesions after stereotactic radiosurgery
- Inflammation around tumour necrosis increases regional cerebral blood volume (rCBV), mimicking progression
- A three-layer apparent diffusion coefficient (ADC) pattern on diffusion-weighted MRI suggests radiation necrosis.
- The combined use of rCBV and DW MRI enables accurate differentiation.

Keywords Radiation necrosis · Stereotactic radiosurgery · Metastatic brain tumour · Diffusion-weighted imaging · Perfusion-weighted imaging

Introduction

An increase in the size of enhancing lesions on follow-up MRI after stereotactic radiosurgery (SRS) is well documented [1, 2]. This phenomenon causes management dilemmas for physicians who interpret any increase in lesion size as cancer progression based on the conventional concept of tumour treatment response evaluation [3, 4].

Patel et al. [3] reported that approximately one-third of SRS-treated lesions increased in size during follow-up. However, only 10 out of 120 patients (8 %) required salvage surgery for lesion progression, and the vast majority of lesion size increases were asymptomatic and required only observation. The increased size of enhancing lesions after SRS is often associated with an exaggerated immune response against radiation, and this exaggerated immune response may result in improved cancer survival and control [3, 5, 6].

Radiation-induced changes mostly result from injury to the small vessels, such as hyalinisation, fibrinoid necrosis and

J. Cha · S. T. Kim (✉) · H.-J. Kim · H. J. Kim · B.-j. Kim ·
P. Jeon · K. H. Kim · H. S. Byun
Department of Radiology and Center for Imaging Science,
Samsung Medical Center,
Sungkyunkwan University School of Medicine,
50, Irwon-dong, Gangnam-gu,
Seoul 135-710, Republic of Korea
e-mail: st7.kim@samsung.com

spontaneous thrombosis [7]. Other causes of radiation necrosis are direct injury to glial parenchymal elements and immunological reactivity secondary to allergic hypersensitivity [7, 8]. Central nervous system tissue is highly responsive to ionising radiation, and the induction of cytokines is prominent in radiation-induced cellular responses, resulting in local neuroimmune and inflammatory reactions [8]. An experimental study showed the induction of tumour necrosis factor (TNF)- α gene expression, which persisted for 2–3 months following mouse brain irradiation (25 Gy) and was followed by persistent gene overexpression for 6 months [9].

Radiation necrosis of the irradiated brain has various histological features, including coagulation necrosis and liquefaction necrosis [10]. The typical coagulation necrosis shows vascular changes such as fibrinoid necrosis, hyalinisation of the vessel wall and occlusion of the lumen by fibrin thrombi. In the area around typical coagulation necrosis, a zone of active inflammatory response is formed.

Radiation necrosis with markedly increased signal intensity on diffusion-weighted imaging (DWI) and a low apparent diffusion coefficient (ADC) value was reported in a previous study [11, 12]. This is caused by the development of intracellular oedema in the viable tumour cells during the transition to complete necrosis with liquefaction. Also, the low ADC values in radiation necrosis might reflect early necrosis with abundant polymorphonuclear leukocytes, as in purulent fluid, because the high viscosity and inflammatory cellular composition may restrict water diffusion.

Differentiating between tumour progression and radiation necrosis after SRS is often difficult with conventional MRI and even with perfusion-weighted imaging (PWI). The active inflammatory response area around the necrosis area may show increased cerebral blood volume (CBV) and can mimic tumour progression. Based on our clinical experience, we found that analysis of the layering pattern in DWI could help differentiate radiation necrosis and tumour progression. As coagulation necrosis may make a liquefied centre, with a peripheral active inflammatory zone and transition zone in between, the ADC value of the transition zone will be low because of the high viscosity.

Thus, the aim of this study was to evaluate whether DWI findings of radiation necrosis were distinctive compared to those of tumour progression and to evaluate the added value of DWI on PWI.

Materials and methods

Study population

Between January 2008 and January 2012, 21 consecutive patients underwent craniotomy and tumour removal for metastatic brain tumours that increased in size after SRS

and preoperative MRI including DWI and PWI. Images with significant haemorrhage ($n=4$) and motion artefacts ($n=1$) that prevented image analysis were excluded from the study. Finally, 16 consecutive patients (9 men and 7 women with an age range from 38 to 71 years; mean age, 56 years) were included in the study. This retrospective study was approved by the institutional review board in the hospital, and the requirement for informed consent was waived.

The mean interval between SRS and increased size of the lesion was 134 ± 83.4 days with a range of 40 to 311 days. The origins of tumours were as follows: lung adenocarcinoma ($n=8$), lung squamous cell carcinoma ($n=2$), small cell lung cancer ($n=2$), hepatocellular carcinoma ($n=1$), breast cancer ($n=1$), advanced gastric cancer ($n=1$) and sebaceous carcinoma of the eyelid ($n=1$).

MR imaging protocol

Magnetic resonance imaging was obtained at 3.0 T (Achieva, Philips Medical Systems, Best, The Netherlands) with an eight-channel sensitivity-encoding (SENSE) head coil.

Contrast-enhanced axial spin echo T1-weighted imaging was acquired after intravenous injection of contrast material [Dotarem (gadoterate meglumine), Guerbet, Aulnay-sous-Bois, France, 0.1 mmol/kg body weight by power injector] with the following parameters: repetition time/echo time (TR/TE)=500/10 ms; slice thickness = 5 mm; acquisition matrix = 256×226 .

Spin echo EPI DWI (TR/TE=3,000/76 ms, slice thickness = 5 mm, acquisition matrix = 128×128 , b value = 0, 1,000 s/mm²) and dynamic susceptibility contrast (DSC) MR perfusion imaging [TR/TE=1,720/35 ms, flip angle (FA)=40°, slice thickness = 5 mm, acquisition matrix = 128×128 , 50 volumes, acquisition time = 1 min 30 s] were obtained with parameters as described above. All MR sequences were acquired with the same field of view (FOV; 240×240 mm).

ADC map analysis

The layering of ADC values was categorised into three patterns (Fig. 1). The outer boundary of the lesion was considered to be the outer margin of the enhancing area. The one-layer pattern showed matched areas of the decreased ADC value and increased regional cerebral blood volume (rCBV) with enhancement. The two-layer pattern showed a decreased ADC value on the inner layer surrounded by a larger enhancing portion. The three-layer pattern showed an inner layer of increased ADC value and a middle layer of decreased ADC value, which were not enhanced, surrounded by an enhancing portion with increased rCBV.

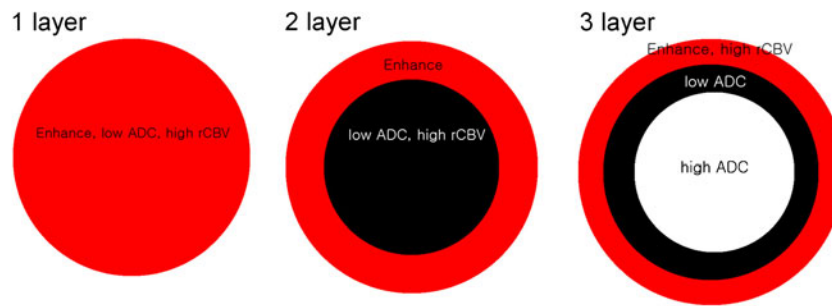


Fig. 1 The layering of apparent diffusion coefficient (ADC) values was categorised into three patterns. The one-layer pattern showed matching of the decreased ADC value, increased regional cerebral blood volume (rCBV) and the enhancing portion. The two-layer pattern showed a decreased ADC value on the inner layer surrounded by

the larger enhancing portion. The three-layer pattern showed an inner layer of increased ADC value and a middle layer of decreased ADC value, which were not enhanced, surrounded by an enhancing portion with increased rCBV

The ADC values were measured on each discernible layer. The minimum ADC was recorded from three regions of interest (ROI; size = 3 mm²).

rCBV map analysis

Dynamic susceptibility contrast perfusion images were processed using a dedicated software package (Nordic ICE; NordicNeuroLab, Bergen, Norway). An rCBV map was generated using an established tracer kinetic model applied to the first-pass data [13]. Gamma variate fitting was applied to avoid a recirculation effect. As described

previously, the dynamic curves were corrected mathematically to reduce contrast agent leakage effects [14]. The rCBV maps were normalised by dividing the rCBV value in the ROI with an unaffected white matter rCBV value defined by a neuroradiologist (J.C.). The maximum rCBV was recorded from three ROIs (size = 3 mm²).

Statistical analysis

Statistical analyses were performed using IBM SPSS Statistics 20 (IBM Corporation, NY, USA). The ADC values and rCBV between the radiation necrosis group

Fig. 2 A 58-year-old woman with metastasis from lung adenocarcinoma who had undergone stereotactic radiosurgery (SRS) 3 months previously. The lesion shows a typical three-layer pattern, which consists of an internal liquefied area surrounded by a transition zone with a low ADC value and reactive inflammatory zone with slightly increased rCBV. The pathological diagnosis was radiation necrosis

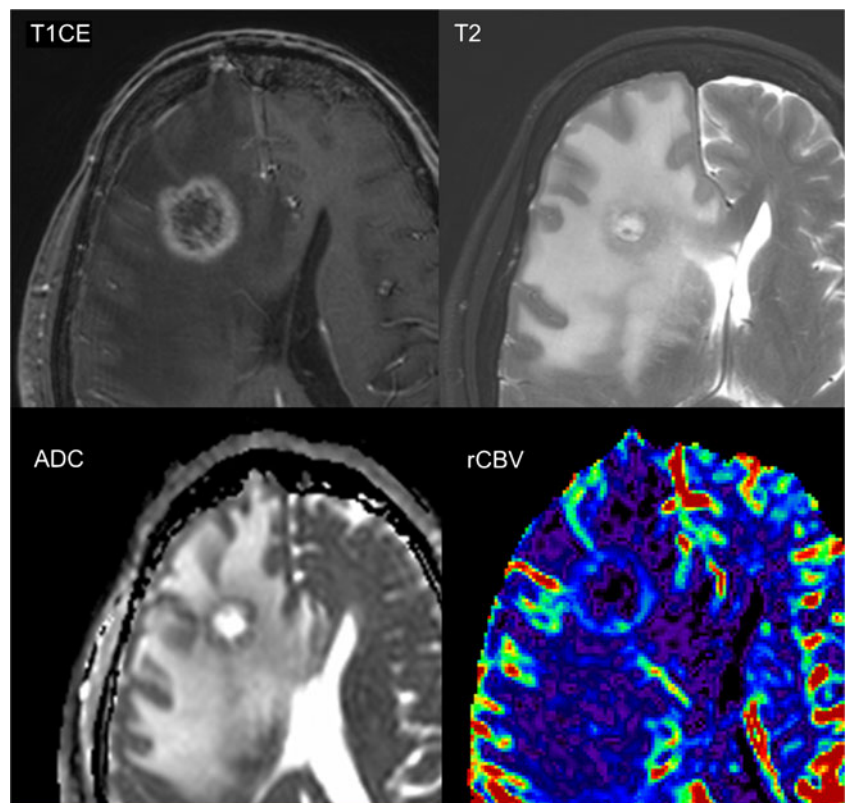
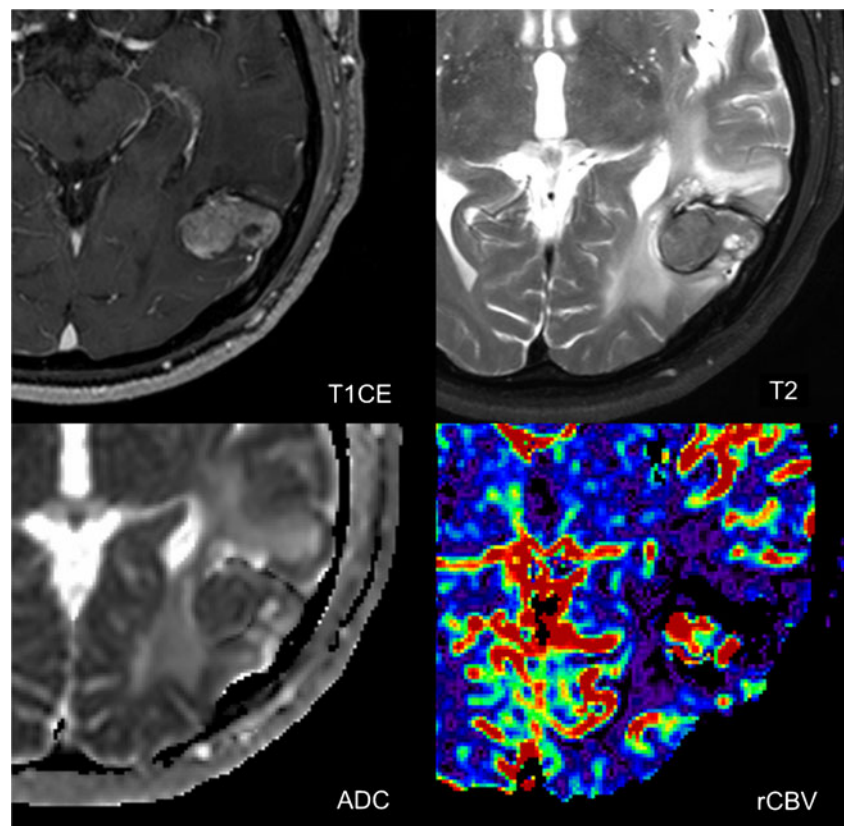


Fig. 3 A 65-year-old man with metastasis from hepatocellular carcinoma who had undergone SRS 5 months previously. The lesion shows a one-layer pattern, which shows matched areas of high cellularity, increased CBV and enhancement. The pathological diagnosis was tumour progression



and the tumour progression group were compared using Fisher's exact test and the Mann-Whitney test. A receiver operating characteristic (ROC) curve was constructed to determine the optimal threshold of rCBV

for differentiating radiation necrosis and tumour progression. For all statistical values, a *P* value less than 0.05 was considered to indicate a statistically significant difference.

Table 1 The patient demographics and layering pattern of the apparent diffusion coefficient (ADC) in the radiation necrosis and tumour progression groups

Index	Age	Sex	Layering pattern of ADC	Group	Pathology
1	71	F	2 layer	Tumour progression	Lung-adeno
2	60	M	2 layer	Tumour progression	Lung-SQ
3	62	M	3 layer	RT necrosis	Lung-SQ
4	60	F	3 layer	RT necrosis	Lung-adeno
5	58	F	3 layer	RT necrosis	Lung-adeno
6	43	M	3 layer	RT necrosis	Lung-adeno
7	65	M	1 layer	Tumour progression	HCC
8	69	F	3 layer	RT necrosis	Lung-adeno
9	69	M	3 layer	Tumour progression	Lung-SCLC
10	47	F	3 layer	RT necrosis	Eyelid- sebaceous carcinoma
11	49	M	2 layer	Tumour progression	Breast
12	56	F	3 layer	RT necrosis	Lung-adeno
13	38	M	3 layer	RT necrosis	Lung-adeno
14	65	M	2 layer	Tumour progression	Lung-adeno
15	42	M	2 layer	Tumour progression	Lung-small cell
16	39	F	3 layer	RT necrosis	AGC

Table 2 The layer of minimum ADC value in the radiation necrosis group and tumour progression group

Minimum ADC	RT necrosis (n=9)	Tumour (n=7)	P value
Layer 1 (inner)	1 (11.1 %)	4 (57.1 %)	0.012
Layer 2 (mid)	8 (88.9 %)	1 (14.3 %)	
Layer 3 (outer)	0 (0 %)	2 (28.6 %)	

Results

Nine cases of radiation necrosis (Fig. 2) and seven cases of tumour progression (Fig. 3) were pathologically confirmed.

All patients in the radiation necrosis group showed the three-layer pattern of ADC (100 % of the radiation necrosis group); however, six patients (85.7 %) in the tumour progression group showed the one- or two-layer pattern ($P=0.001$; Table 1). The minimum ADC was measured at the middle layer in the radiation necrosis group (88.9 %), but in the tumour progression group, the minimum ADC was measured at the inner layer (57.1 %; $P=0.012$; Table 2). There was only one exception having the minimum ADC at the middle layer in the tumour progression group; however,

in that patient, the rCBV was 7.8, which may suggest tumour progression (Fig. 4).

The minimum ADC was smaller in the radiation necrosis group than in the tumour progression group ($655.7 \pm 184.4 \times 10^{-6} \text{ mm}^2/\text{s}$ versus $829.6 \pm 224.5 \times 10^{-6} \text{ mm}^2/\text{s}$, respectively); however, it was not statistically significant ($P=0.138$). rCBV was higher in the tumour progression group than in the radiation necrosis group (6.3 ± 3.2 versus 2.8 ± 1.0 , respectively; $P=0.013$; Table 3). There were no significant differences in terms of the mean values of each ADC layer (inner, middle, outer) in the radiation necrosis group and tumour progression group.

On the ROC curve analysis, the area under the curve (AUC) of rCBV for differentiating tumour progression from radiation necrosis was 0.873 (Fig. 5). If rCBV larger than 2.6 was used to differentiate radiation necrosis and tumour progression, the sensitivity was 100 % but specificity was 56 % owing to an overlapping portion (Fig. 6). If an rCBV larger than 4.1 was used to differentiate radiation necrosis and tumour progression, the sensitivity was 71.4 % and specificity was 100 %. If the diagnostic criterion was set to (1) the lesion with an rCBV larger than 2.6 that did not have the three-layer pattern of ADC or (2) the lesion with an rCBV larger than 4.1, the sensitivity and specificity were 100 %.

Fig. 4 A 69-year-old man with metastasis from small cell lung cancer who had undergone SRS 4 months previously. The lesion shows the three-layer pattern of ADC, which mimics radiation necrosis. However, the rCBV of the enhancing portion is highly elevated. The pathological diagnosis was tumour progression

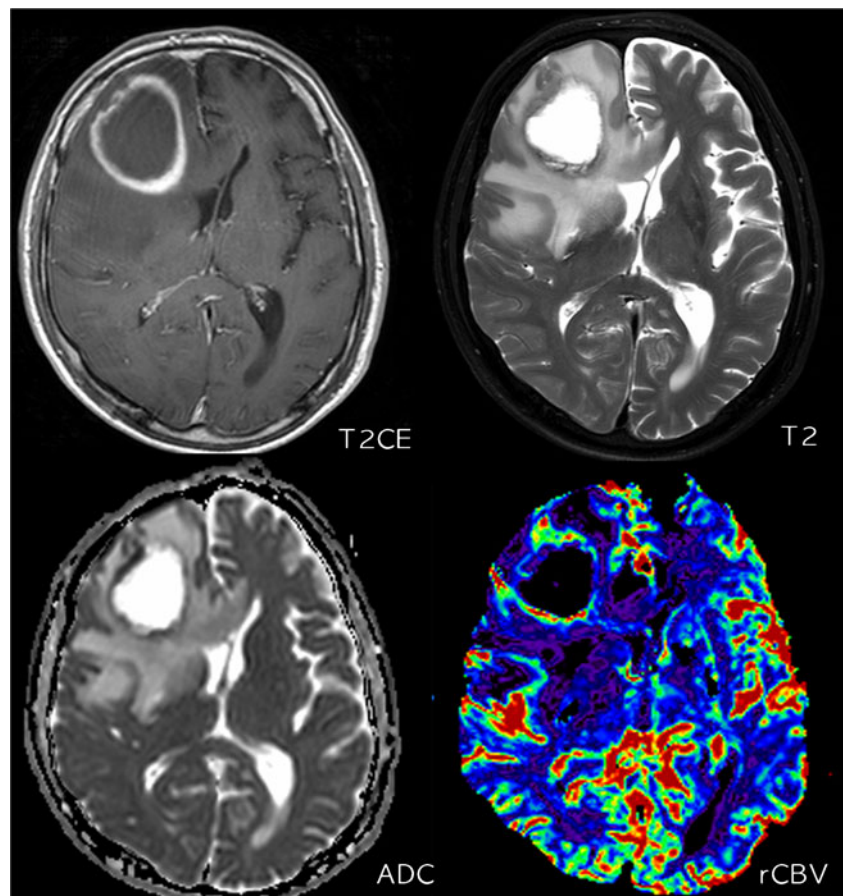


Table 3 The mean ADC value ($\times 10^{-6}$ mm²/s) of each layer, the mean of the minimum ADC and maximum rCBV in the radiation necrosis group and tumour progression group

	RT necrosis (<i>n</i> =9)	Tumour (<i>n</i> =7)	<i>P</i> value
ADC inner	2,011.3±733.0	1,393.6±997.5 (<i>n</i> =6) ^a	0.262
ADC mid	753.6±352.2	616.4 (<i>n</i> =1) ^a	0.862
ADC outer	1,245.6±103.5	1,173.7±253.2	0.791
Min ADC	655.7±184.4	829.6±224.5	0.138
rCBV	2.8±1.0	6.3±3.2	0.013

Numbers represent mean ± standard deviation

^aOnly the lesions that have an inner or middle layer were included

Discussion

Approximately one third of lesions treated with SRS increased in size during follow-up [3]. Increasing initial size is associated with a higher probability of a post-SRS increase in lesion size [3, 15]. Male sex and mean voxel dose <37 Gy are associated with a higher probability of a post-SRS increase in lesion size [3]. With regard to the timing of lesion growth, most lesions increase in size 3–6 months post-SRS. However, this enlargement can start as early as 6 weeks post-SRS and may not reach peak volume until 15 months post-SRS [3]. In this study, the time interval between SRS and increased size of the lesion was 134 ± 83.4 days (range from 40 to 311 days), which was consistent with previous reports.

Patel et al. [3] found that for those patients in whom all lesions increased in size, median survival was >18.4 months

compared with 16.4 months for patients whose lesions showed mixed responses and 9.5 months for patients whose lesions all remained stable or decreased in size. They said the post-SRS lesional growth may not represent tumour regrowth at all but rather a brisk reactive immune response that is related to or causes apparent lesional growth on MR imaging; however, not all cases were pathologically confirmed.

Diffusion-weighted imaging has been used to differentiate brain abscess from necrotic tumour [12, 16]. Contrary to purulent fluid in the brain abscess, which shows diffusion

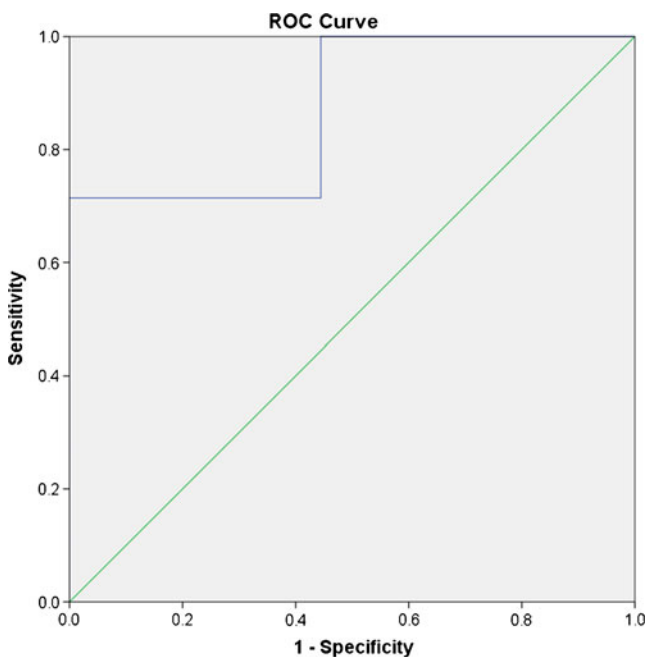


Fig. 5 Receiver-operating characteristic (ROC) curves of rCBV for differentiating tumour progression from radiation necrosis. Diagonal line = 50 % of the area under the ROC curve

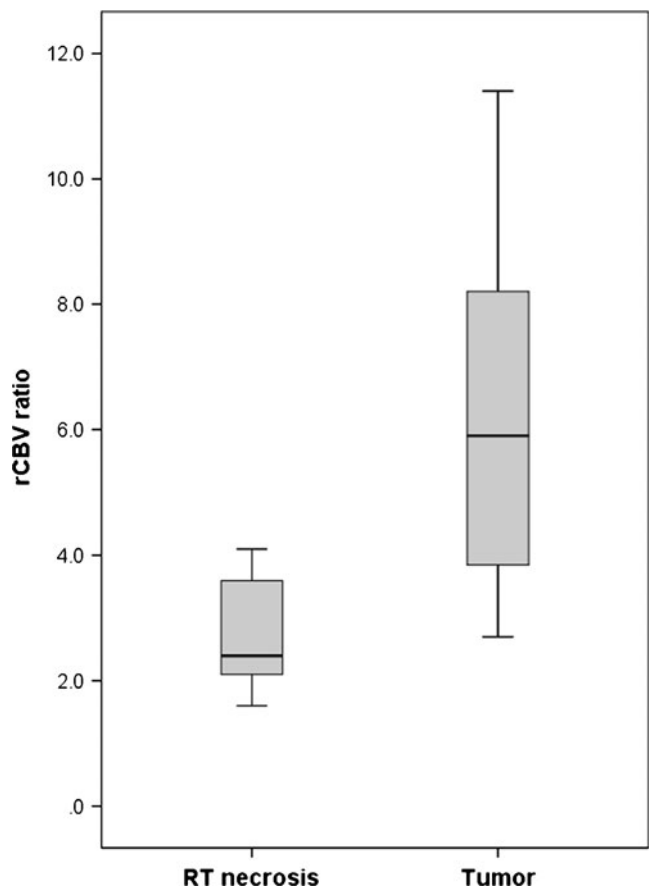


Fig. 6 Box-and-whisker chart shows rCBV (*B*) comparison of RT necrosis and tumour progression

restriction, necrotic areas in primary and metastatic tumours are usually more haemorrhagic, less viscous and less cellular, and therefore do not show diffusion restriction.

It is also well established that therapeutic radiation causes vasculopathy and necrosis in treated tissue. In cases of radiation necrosis of the brain, the necrotic areas show coagulation necrosis and liquefied softening necrosis [10]. In the area around the liquefied centre, more active inflammatory responses are formed with lymphocytes and macrophages as a partial rim of the reactive zone and surrounded by reactive gliosis and demyelination [3, 10]. Histologically, radiation-induced injury has been well-described as an area of necrosis surrounded by a robust inflammatory cell infiltrate that may also contain some tumour cells [17, 18]. Areas of sterile coagulation necrosis may contain creamy pus-like material with abundant polymorphonuclear leukocytes [19]; therefore, radiation necrosis may show diffusion restriction, that is, low ADC values. In previous reports of radiation necrosis of metastasis with low ADC values, the authors suggested that this low ADC value could be explained by the development of intracellular oedema in the viable tumour cells during the transition to complete necrosis with liquefaction [11, 12, 20, 21]. Therefore, mature radiation necrosis may show a three-layer pattern: an inner layer of complete necrosis with liquefaction that shows an increased ADC value, a middle layer of transition zone with a low ADC value and an outer layer of the active inflammatory zone with increased rCBV.

In previous studies, a lower ADC value was considered to indicate higher cellularity in a recurrent tumour [11, 22]. However, the range of the ADC values of a tumour is about $800\text{--}1,200 \times 10^{-6} \text{ mm}^2/\text{s}$. In their study, Toh et al. [23] showed that the mean ADC values of the enhancing rim in abscess, glioblastoma and metastasis were 691, 1,268 and $1,271 \times 10^{-6} \text{ mm}^2/\text{s}$, respectively. The ‘infarct-like’ extremely low ADC value of about $600 \times 10^{-6} \text{ mm}^2/\text{s}$ may not be achieved by tumour and may only be achieved by infarction, abscess or radiation necrosis. Also, if the low ADC value portion was a viable tumour portion, the lesion should show contrast enhancement; however, in this study, the ‘infarct-like’ low ADC portion located in the middle layer did not show contrast enhancement.

The most widely used technique for a perfusion study is to evaluate the rCBV from DSC MR perfusion imaging [22, 24]. With an increment of vascularity in tumours, new vessels and damaged mature vessels are permeable to contrast agents, unlike vessels in the normal brain. Measurement of the rCBV reliably correlates with tumour grade and histological findings of increased tumour vascularity, particularly in gliomas [25]. rCBV can be used to differentiate between a radiation-induced change and tumour progression by estimating the regional CBV after radiosurgery. A decrease in rCBV values indicates a tumour response to

therapy regardless of increases in tumour volume, which might be due to radiation-induced oedema and blood–brain barrier disruption, and necrosis as seen in a follow-up MRI study after radiosurgery. If an increment of rCBV in the enhancing component of the mass after radiosurgery appears on follow-up MRI, this finding may be considered indicative of tumour progression [26, 27].

In the area around the liquefied centre in radiation necrosis, there are more active inflammatory responses, resulting in some degree of increased rCBV. This results in a thin rim of increased rCBV on the peripheral portion of the necrotic area (Fig. 2); therefore, there is significant overlap of rCBV between radiation necrosis and tumour progression [28]. In our study, the specificity of $\text{rCBV} > 2.6$ for differentiating radiation necrosis and tumour progression was only 56 %. Also, the sensitivity of $\text{rCBV} > 4.1$ for differentiating radiation necrosis and tumour progression was 71.4 %. On the other hand, the three-layer pattern of ADC with a low ADC on the middle layer was highly specific for radiation necrosis. If the lesion with the three-layer pattern of ADC with moderately increased rCBV (2.6–4.1) was excluded from $\text{rCBV} > 2.6$, the sensitivity and specificity were increased to 100 %.

Our study has several limitations. Because of the small number of patients, a selection bias may have occurred. Next, pathological matching was not performed on each layer of the ADC. Also, the primary tumour site was heterogeneous; thus, the nature of the primary tumour may act as a bias.

In conclusion, the sensitivity and specificity of rCBV in diagnosing tumour progression is not high owing to an overlapping portion; therefore, the differentiation of tumour progression from radiation necrosis is often difficult. The presence of the three-layer pattern of ADC was highly specific for radiation necrosis. Therefore, a combination of ADC with rCBV may have added value in the correct differentiation of tumour progression from radiation necrosis.

References

1. Huber PE, Hawighorst H, Fuss M, van Kaick G, Wannemacher MF, Debus J (2001) Transient enlargement of contrast uptake on MRI after linear accelerator (LINAC) stereotactic radiosurgery for brain metastases. *Int J Radiat Oncol Biol Phys* 49:1339–1349
2. Da Silva AN, Nagayama K, Schlesinger D, Sheehan JP (2009) Early brain tumor metastasis reduction following Gamma Knife surgery. *J Neurosurg* 110:547–552
3. Patel TR, McHugh BJ, Bi WL, Minja FJ, Knisely JP, Chiang VL (2011) A comprehensive review of MR imaging changes following radiosurgery to 500 brain metastases. *AJNR Am J Neuroradiol* 32:1885–1892
4. Eisenhauer EA, Therasse P, Bogaerts J et al (2009) New response evaluation criteria in solid tumours: revised RECIST guideline (version 1.1). *Eur J Cancer* 45:228–247

5. Vannucci L (2010) To suppress to rescue? Changing the approach for recalling anticancer immune responses. *Front Biosci (Schol Ed)* 2:1189–1197
6. Hamai A, Benlalam H, Meslin F et al (2010) Immune surveillance of human cancer: if the cytotoxic T-lymphocytes play the music, does the tumoral system call the tune? *Tissue Antigens* 75:1–8
7. Rabin BM, Meyer JR, Berlin JW, Marymount MH, Palka PS, Russell EJ (1996) Radiation-induced changes in the central nervous system and head and neck. *Radiographics* 16:1055–1072
8. Gourmelon P, Marquette C, Agay D, Mathieu J, Clarencon D (2005) Involvement of the central nervous system in radiation-induced multi-organ dysfunction and/or failure. *BJR Suppl/BIR* 27:62–68
9. Chiang CS, Hong JH, Stalder A, Sun JR, Withers HR, McBride WH (1997) Delayed molecular responses to brain irradiation. *Int J Radiat Biol* 72:45–53
10. Yoshii Y (2008) Pathological review of late cerebral radionecrosis. *Brain Tumor Pathol* 25:51–58
11. Asao C, Korogi Y, Kitajima M et al (2005) Diffusion-weighted imaging of radiation-induced brain injury for differentiation from tumor recurrence. *AJNR Am J Neuroradiol* 26:1455–1460
12. Tung GA, Evangelista P, Rogg JM, Duncan JA 3rd (2001) Diffusion-weighted MR imaging of rim-enhancing brain masses: is markedly decreased water diffusion specific for brain abscess? *AJR. Am J Roentgenol* 177:709–712
13. Ostergaard L, Weisskoff RM, Chesler DA, Gyldensted C, Rosen BR (1996) High resolution measurement of cerebral blood flow using intravascular tracer bolus passages. Part I: Mathematical approach and statistical analysis. *Magn Reson Med: Off J Soc Magn Reson Med/Soc Magn Reson Med* 36:715–725
14. Boxerman JL, Schmainda KM, Weisskoff RM (2006) Relative cerebral blood volume maps corrected for contrast agent extravasation significantly correlate with glioma tumor grade, whereas uncorrected maps do not. *AJNR Am J Neuroradiol* 27:859–867
15. Pan HC, Sheehan J, Stroila M, Steiner M, Steiner L (2005) Gamma knife surgery for brain metastases from lung cancer. *J Neurosurg* 102:128–133
16. Desprechins B, Stadnik T, Koerts G, Shabana W, Breucq C, Osteaux M (1999) Use of diffusion-weighted MR imaging in differential diagnosis between intracerebral necrotic tumors and cerebral abscesses. *AJNR Am J Neuroradiol* 20:1252–1257
17. Jagannathan J, Bourne TD, Schlesinger D et al (2010) Clinical and pathological characteristics of brain metastasis resected after failed radiosurgery. *Neurosurgery* 66:208–217
18. Oh BC, Pagnini PG, Wang MY et al (2007) Stereotactic radiosurgery: adjacent tissue injury and response after high-dose single fraction radiation: Part I—Histology, imaging, and molecular events. *Neurosurgery* 60:31–44, discussion 44–35
19. Monabati A, Kumar PV, Kamkarpour A (2000) Intraoperative cytodagnosis of metastatic brain tumors confused clinically with brain abscess. A report of three cases. *Acta Cytol* 44:437–441
20. Holtas S, Geijer B, Stromblad LG, Maly-Sundgren P, Burtscher IM (2000) A ring-enhancing metastasis with central high signal on diffusion-weighted imaging and low apparent diffusion coefficients. *Neuroradiology* 42:824–827
21. Biousse V, Newman NJ, Hunter SB, Hudgins PA (2003) Diffusion weighted imaging in radiation necrosis. *J Neurol Neurosurg Psychiatry* 74:382–384
22. Kang TW, Kim ST, Byun HS et al (2009) Morphological and functional MRI, MRS, perfusion and diffusion changes after radiosurgery of brain metastasis. *Eur J Radiol* 72:370–380
23. Toh CH, Wei KC, Ng SH, Wan YL, Lin CP, Castillo M (2011) Differentiation of brain abscesses from necrotic glioblastomas and cystic metastatic brain tumors with diffusion tensor imaging. *AJNR Am J Neuroradiol* 32:1646–1651
24. Cha S (2006) Update on brain tumor imaging: from anatomy to physiology. *AJNR Am J Neuroradiol* 27:475–487
25. Wong JC, Provenzale JM, Petrella JR (2000) Perfusion MR imaging of brain neoplasms. *AJR Am J Roentgenol* 174:1147–1157
26. Essig M, Waschkies M, Wenz F, Debus J, Hentrich HR, Knopp MV (2003) Assessment of brain metastases with dynamic susceptibility-weighted contrast-enhanced MR imaging: initial results. *Radiology* 228:193–199
27. Mitsuya K, Nakasu Y, Horiguchi S et al (2010) Perfusion weighted magnetic resonance imaging to distinguish the recurrence of metastatic brain tumors from radiation necrosis after stereotactic radiosurgery. *J Neurooncol* 99:81–88
28. Jain R, Narang J, Schultz L et al (2011) Permeability estimates in histopathology-proved treatment-induced necrosis using perfusion CT: can these add to other perfusion parameters in differentiating from recurrent/progressive tumors? *AJNR Am J Neuroradiol* 32:658–663